THE JOURNAL OF PHYSICAL CHEMISTRY A

pubs.acs.org/JPCA Article

Theoretical Investigations of Rate Coefficients for H + O_3 and HO_2 + O Reactions on a Full-Dimensional Potential Energy Surface

Published as part of The Journal of Physical Chemistry virtual special issue "Machine Learning in Physical Chemistry".

Junxiang Zuo,[‖] Qixin Chen,[‖] Xixi Hu,* Hua Guo, and Daiqian Xie*

Cite This: *J. Phys. Chem. A* 2020, 124, 6427−6437 Read Online

ACCESS | Metrics & More | Article Recommendations

ABSTRACT: In this work, a machine learning method is used to construct a high-fidelity multichannel global reactive potential energy surface (PES) for the HO_3 system from 21452 high-level *ab initio* calculations at the explicitly correlated multireference configuration interaction (MRCI-F12) level of theory. The permutation invariance of the PES with respect to the three identical oxygen atoms is enforced using permutation invariant polynomials (PIPs) in the input layer of a neural network (NN). This PIP-NN representation is highly faithful to the *ab initio* points, with a root-mean-square error of 0.20 kcal/mol. Using this PES, the kinetics of H + O_3 → OH + O_2 (R1) and HO_2 + O → OH + O_2 (R2) reactions were investigated using a quasi-classical trajectory method over a wide temperature range (200−2000 K). It was found that the calculated thermal rate coefficients of R1 and R2, exhibiting positive and negative temperature dependences, respectively, are in reasonably good agreement with most experimental measured values. These temperature dependences can be attributed to the presence and absence of an entrance channel potential barrier.

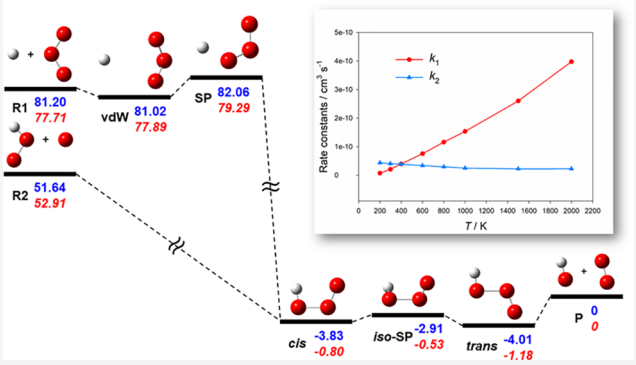

I. INTRODUCTION

The hydrogen trioxide (HO_3), serving as a transient intermediate in several important gas-phase reactions, has long been postulated to play an important role in astrochemistry, atmospheric chemistry, and combustion.[1−4] The following two major reactions

$$H(^2S) + O_3(X^1A_1) \rightarrow OH(X^2\Pi) + O_2(X^3\Sigma_g^-)$$

$$\Delta H = -77.72 \text{ kcal/mol} \quad \text{(R1)}$$

$$HO_2(X^2A'') + O(^3P) \rightarrow OH(X^2\Pi) + O_2(X^3\Sigma_g^-)$$

$$\Delta H = -53.77 \text{ kcal/mol} \quad \text{(R2)}$$

proceed on the HO_3 ground state potential energy surface (PES). Both reactions are highly exoergic. Reaction R1 is of fundamental importance in atmospheric airglow and generates vibrationally excited OH radicals which are the source of the Meinel bands in the upper atmosphere.[5] The second reaction (R2) is a major odd oxygen destruction pathway in the upper stratosphere and mesosphere and, along with R1, plays an important role in controlling the partitioning among H, HO_2, and OH radicals in the upper atmosphere.[6] In addition to its importance in atmospheric chemistry, R2 is a chain breaking step in H_2/O_2 combustion.[2] Kinetic modeling showed sensitivity to both the forward and reverse directions of the reaction.[7] An accurate determination of the rate coefficients for these reactions and their temperature dependence over a larger temperature range is essential for related atmospheric and combustion modeling.

Reactions R1 and R2 have been the subject of many experimental studies in the past several decades. The first experimental measurements of the rate coefficient for R1 (k_1) were carried out by Phillips and Schiff in 1962 using discharge flow mass spectrometry,[8] and the value at 298 K, $(2.6 \pm 0.5) \times 10^{-11}$ cm^3/s, was obtained. Since then, k_1 has been studied over the temperature range from 196 to 638 K using several techniques,[9−12] which indicated a positive temperature dependence. However, there are significant uncertainties among the measured rate coefficients. At room temperature,

Received: May 14, 2020
Revised: June 23, 2020
Published: July 19, 2020

https://dx.doi.org/10.1021/acs.jpca.0c04321
J. Phys. Chem. A 2020, 124, 6427−6437

for example, the difference between those reported by Lee et al.[10] ($\sim 2.85 \times 10^{-11}$ cm^3/s) and by Greenblatt et al.[12] ($\sim 1.5 \times 10^{-11}$ cm^3/s) is almost a factor of 2. For reaction R2, there has also been a great deal of interest in kinetics experiments.[13−23] Most of the investigators focused on the rate coefficient of R2 (k_2) at around 298 K and the measured values range from 3.10×10^{-11} to 7.00×10^{-11} cm^3/s,[15−18,20−22] indicating again uncertainties in the measurements. Nicovich and Wine[23] reported results of pulse laser photolysis measurements over the temperature range 266−391 K, and k_2 has a negative temperature dependence. The absolute uncertainty in k_2 was estimated to be ±22%. To date, there have been only two experimental investigations of k_2 at high temperatures.[13,14]

Theoretically, a plethora of investigations of HO_3 have been reported. However, the focus of many efforts was placed on the structural properties of the HO_3 complexes and their relative stability, because of its perceived role as an OH sink in the atmosphere.[3,24−39] Varandas et al.[40] developed the first global PES for the ground state HO_3 fitted to UCISD/6-311G++(d, p) points using the double many-body expansion (DMBE) method with a root-mean-square fitting error of 5.33 kcal/mol. This DMBE I PES showed a submerged barrier for R1 in the entrance channel and no barrier in the R2 entrance channel. It also predicted a metastable HO_3 well with a nonplanar geometry, while experimental measurements[41−43] show that HO_3 is planar. Both full-dimensional quasi-classical trajectory (QCT) and three-dimensional quantum dynamic (QD) calculations were reported on the DMBE I PES for R1 and R2.[44−47] However, the quantum rate coefficients for both R1[45] and R2[47] are smaller by several times than the QCT results due presumably to the reduced dimensionality in the QD treatment, and both deviated from experiment. Later, an improved HO_3 PES, named DMBE II PES, was constructed by fitting 5038 QCISD(T)/CBS points in the $HO_3 \rightarrow OH + O_2$ region, with a root-mean-square fitting error of 0.75 kcal/mol.[33] It was combined with the DMBE I PES by using a switching function. It improves the description of HO_3 with two stable planar isomers. However, *cis*-HO_3 lying 6.48 kcal/mol below the OH + O_2 dissociation limit is more stable than the *trans* one, while experiment[48] suggests that *trans*-HO_3 is the more stable conformer. Furthermore, the OH + O_2 recombination reaction to *cis*-HO_3 has a barrier of 1.36 kcal/mol, which is inconsistent with the later experimental observation which indicated this process has no barrier.[43] The two DMBE PESs were also used to investigate the dynamics of R2 with a QCT method. The calculated rate coefficients on both PESs have similar trends,[49,50] as expected since these exoergic reactions are mostly controlled by the entrance channel potentials. In addition, Setokuchi et al.[34] investigated the minimum energy path (MEP) for R2 using a multireference second-order Møller−Plesset perturbation (MRMP2) method with the TZV(2df, 2p) basis sets, and their calculated rate coefficients based on the microcanonical variational transition state theory are within the experimental upper and lower limits in the range of 200−400 K but exhibit a slightly larger negative temperature dependence than the recommended values[51] by NASA. In 2008, Braams and Yu[30] constructed an analytical PES by fitting 28000 points that were sampled mostly over the region for the $HO_3 \rightarrow OH + O_2$ reaction and calculated using the density functional theory with the Hamprecht−Cohen−Tozer−Handy (HCTH) functional and the aug-cc-pVTZ basis set. However, this PES does not have enough points in two reactant channels and the calculated vibrational frequencies of the HO_3 intermediates have large discrepancies with experiment,[29] suggesting major deficiencies. In order to better understand the aforementioned kinetic experiments and dynamics, it is imperative to obtain a more accurate global PES for the HO_3 system extending to all three arrangement channels and perform full-dimensional dynamical investigations for various reactive processes.

With three heavy atoms involved and strong multireference character, the *ab initio* calculations of this system are extremely challenging.[39] Recently, we have reported a full-dimensional PES for the OH + $O_2 \leftrightarrow HO_3$ association reaction based on 2087 *ab initio* points at the MRCI-F12/VDZ-F12 level.[52] The dissociation energy is in reasonable agreement with known values. The low-lying vibrational energy levels of HO_3/DO_3 isomers calculated on this PES are in very good agreement with the available experiments. However, that PES does not extend to the reactant channels of R1 and R2. In this work, we report a new global multichannel PES that is capable of describing all three channels of OH + O_2, H + O_3, and HO_2 + O, at the same level of theory. This is a challenge because this PES has to cover a large energy span due to the high exoergicity of the reactions but at the same time reproduce isomers of the HO_3 complex with a small difference of energy. To this end, we have used a machine learning method based on neural networks, which provide a highly flexible representation of the global multichannel PES.[53−55] Permutation symmetry of the PES is enforced using symmetry functions as the input. The new PES is further employed for QCT calculations to obtain the rate coefficients for reactions R1 and R2 over a wide temperature range, with reasonably satisfactory agreement with available experimental data. The paper is organized as follows. Section II outlines the *ab initio* calculations, fitting approach, and QCT calculations. The properties of PES and kinetic studies are present in section III. Finally, the conclusions are given in section IV.

II. METHODS

II.A. *Ab Initio* Calculations. *Ab initio* calculations at all geometries were performed with the quantum chemical program package MOLPRO 2015.1.0.[56] Following our recent work,[52] the same multireference method was used to map out the global ground state HO_3 PES. Briefly, dynamically weighted state-averaged complete active space self-consistent field (DW-SA-CASSCF) calculations[57,58] were first performed based on initial Hartree−Fock wave functions. This is followed by explicitly correlated multireference configuration interaction (MRCI-F12) calculations[59] with the VDZ-F12 basis set[60] to capture the dynamical correlation. The calculations using this basis set are already extremely demanding computationally, and no larger basis set was attempted. Fortunately, the explicitly correlated basis set is known to converge rapidly to the complete basis set limit, and tests in our earlier work showed reasonable convergence.[52] The active space used in the CASSCF calculations includes 13 electrons in 10 orbitals with 2s orbitals of O atoms closed, while the full-valence active space was used in subsequent MRCI calculations. Specially, eight-state ($4^2A' + 4^2A''$) DW-SA-CASSCF calculations were carried out with the weighting function $w(i) = [2/(\exp(-\beta\Delta_i) + \exp(\beta\Delta_i))]^2$.[57,58] Here, Δ_i is the energy of the ith excited state relative to the ground state and $\beta^{-1} = 3.0$ eV. In our earlier work,[52] the rotated reference Davidson correction (Q)[61] was included in the *ab initio* calculation, and the correlation energy (roughly defined as the difference between the

https://dx.doi.org/10.1021/acs.jpca.0c04321
J. Phys. Chem. A 2020, 124, 6427−6437

CASSCF energy and the MRCI(Q)-F12 value) was scaled by a factor of 1.059. It is important to point out that the scaling scheme used in this work is different from that in our earlier work.[52] To give a balanced description of the well depths, isomerization path, and reaction energies for this system, we scaled the energy (the difference between the CASSCF reference and the MRCI-F12 value) by a factor of 1.3282. This scaling factor was optimized by reproducing the experimental reaction energies for both R1 and R2.

II.B. Construction of PES. To construct an accurate full-dimensional global HO_3 PES with acceptable computational costs, an appropriate and efficient sampling scheme covering all relevant configuration regions is crucial. The ranges of geometry configurations and energies were determined according to the stationary points along the reaction paths. In this work, we pay particular attention to the H + O_3, HO_2 + O, and OH + O_2 reaction channels and the HOOO interaction region. Only points with energies lower than 6.0 eV relative to the global minimum of the PES have been included. We carefully select the bond lengths, bond angles, and dihedral angles around the stationary points and obtained the first batch of points for PES fit. On this primitive PES, classical trajectories were launched to generate new points. An additional point is added if it satisfies the geometric criterion that the Euclidean distances from all existing points are greater than 0.2 Å. This process was repeated until the PES achieves convergence. A total of 21452 *ab initio* points has been used in the final fit of the global PES.

The PES was fit using a machine learning method. Specifically, an artificial neural network (NN) with low-order permutation invariant polynomials (PIPs) in the input layer, namely, the PIP-NN method,[62,63] was used. The use of NNs allows an accurate representation of any real analytic function with complicated topological features, such as the PES for the HO_3 system. In this work, the NN consists of one input layer, two hidden layers, and an output layer, which are interconnected by neurons. The value of the kth neuron in the ith hidden layer can be defined as

$$y_k^i = f_i\left(b_k^i + \sum_{j=1}^{N_{i-1}} w_{jk}^i y_j^{i-1}\right), \quad i = 1, 2 \tag{1}$$

where f_i is a transfer function (hyperbolic tangent) for the hidden layer, N_{i-1} is the number of neurons, b_k^i are biases of the neurons, and w_{jk}^i are weights connecting the jth neuron in the $(i-1)$th layer and the kth neuron in the ith layer. The output layer, which gives the potential energy through a linear transfer function, is analogously expressed as a single neuron in the final layer.

To enforce the permutation symmetry of the three identical O atoms in HO_3, which is of great importance for an accurate representation of the PES, the PIPs were constructed in the following form[64]

$$G = \hat{S}\prod_{i<j}^{4} p_{ij}^{l_{ij}} \tag{2}$$

where $p_{ij} = \exp(-\alpha r_{ij})$ is the Morse-like monomial in order of l_{ij} with a = 0.4 Bohr^{-1} and r_{ij} is the internuclear distance between atoms i and j. $\hat{S}$ is the symmetrization operator consisting of all possible nuclear permutation operations in this system. In total, 22 PIPs up to the third order were included in the input layer. The standard feed-forward NN with two hidden layers of 50 and 80 neurons was performed utilizing the Levenberg−Marquardt algorithm.[65] The "early stopping" method[54] was used to avoid overfitting, and the root-mean-square error (RMSE) was defined by $\mathrm{RMSE} = [\sum_{i=1}^{N_{\mathrm{data}}}(E_i^{\mathrm{fit}} - E_i^{ab\ initio})^2/N_{\mathrm{data}}]^{1/2}$ to evaluate the quality of each fitting. In the NN fitting, the points were randomly divided into the training (90%), validation (5%), and testing (5%) sets. One hundred different NN training calculations were performed, and the final PIP-NN PES was chosen as the average of the three best fits in order to further reduce the random errors.

II.C. QCT Calculations. In this work, the QCT calculations for both the H + O_3 and HO_2 + O reactions were carried out utilizing the VENUS program package.[66,67] The calculation strategies are essentially the same as ones in our recent work.[68,69] Here we only make a brief explanation on the simulation parameters. Batches of 10^4−10^5 trajectories have been run on the new PIP-NN PES. The maximal impact parameter $b_{\max}$ was chosen by performing a small set of trajectories with trial values. Here, $b_{\max}$ was determined to be 3.0 and 5.5 Å for H + O_3 and HO_2 + O reactions, respectively, over the entire temperatures range of 200−2000 K. All trajectories in QCT calculations are started from a 10 Å separation between reactants (H + O_3 or HO_2 + O). The translational energy and initial ro-vibrational energies of reactants were sampled according to the Boltzmann distribution at each temperature. Reactive or nonreactive trajectories are terminated when the products or reactants reach a separation of 8.0 or 10.5 Å, respectively. Long trajectories with a propagation time greater than 10.0 ps, which are very few in number, were halted and excluded from the final results. To converge the energy of most trajectories within 0.01 kcal/mol, the propagation time step was selected to be 0.1 fs. A so-called "passive" method[70] was applied to correct the product zero-point energy (ZPE) violation by discarding both reactive trajectories with vibrational energies below the ZPEs of the products and nonreactive trajectories with vibrational energies less than the ZPEs of the reactants.

As usual, the thermal rate coefficients can be calculated by the expression

$$k(T) = g_e\left(\frac{8k_BT}{\pi\mu}\right)^{1/2}\pi b_{\max}^2\frac{N_r}{N_{\mathrm{tot}}} \tag{3}$$

in which N_r and N_{tot} are the numbers of reactive and total trajectories. k_B is the Boltzmann constant, and μ is the reduced mass of the reactants. The electronic degeneracy factor (g_e) is chosen to be 1 for the H + O_3 reaction, and $g_e = 1/(5 + 3e^{-158.5\ \mathrm{cm}^{-1}/k_BT} + e^{-226.5\ \mathrm{cm}^{-1}/k_BT})$ for the HO_2 + O reaction to account for spin−orbit splitting of the triplet O atom. The statistical error is given by $\sigma = [(N_{\mathrm{tot}} - N_r)/(N_{\mathrm{tot}}N_r)]^{1/2}$.

III. RESULTS AND DISCUSSION

III.A. Properties of PES. In this work, a total of 21452 *ab initio* points at the level of MRCI-F12/VDZ-F12 are used to fit the global multichannel PES. The RMSEs of the training/validation/testing sets for the three best PES fits are 0.19/0.47/0.65, 0.21/0.49/0.52, and 0.21/0.53/0.54 kcal/mol, respectively. The overall RMSE of the averaged PIP-NN PES is only 0.20 kcal/mol with a maximum deviation of 4.83 kcal/mol. The distribution of *ab initio* points as a function of the potential energy is shown in Figure 1a, while fitting errors of all

https://dx.doi.org/10.1021/acs.jpca.0c04321
J. Phys. Chem. A 2020, 124, 6427−6437

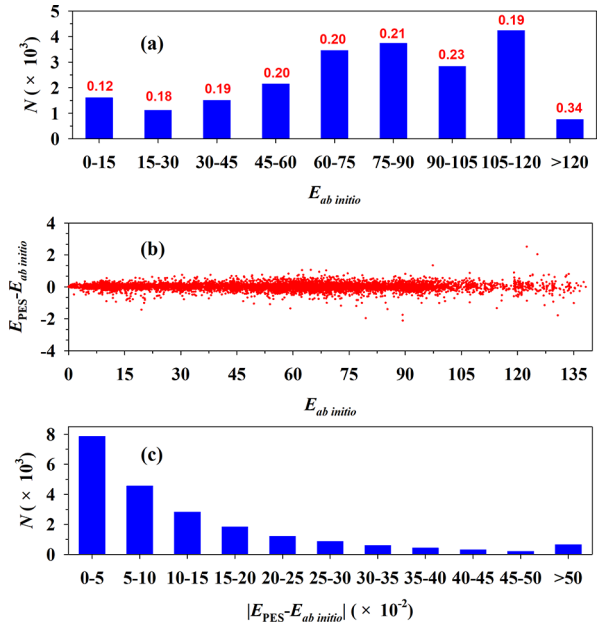

Figure 1. (a) Distribution of *ab initio* points. The red number is the RMSE of the points in each energy range. (b) Fitting errors as a function of the *ab initio* energy. (c) Distribution of the fitting errors for all points. Energies are in kcal/mol with respect to the *trans*-HO_3 complex.

ab initio data and their distribution are presented in Figure 1b and c. The RMSEs in various energy ranges are marked in Figure 1a using red numbers. It is clear that the fitting errors are evenly distributed in the entire energy range of 0−140 kcal/mol. About 8000 points have fitting errors less than 0.05 kcal/mol and ∼5000 points within 0.05−0.10 kcal/mol. The errors for almost 80% of the points are smaller than 0.20 kcal/mol, indicating a high fidelity fitting of the PES using the PIP-NN approach.

Figure 2 displays the schematic of the ground state $HO_3(^2A'')$ PES, including all calculated geometries and energies of stationary points along both the H + O_3 → OH + O_2 (R1) and HO_2 + O → OH + O_2 (R2) reaction pathways. The relative energies of stationary points in the relevant region for the HO_3 → OH + O_2 process are in good agreement with the results obtained from our earlier PES[52] but differ qualitatively and quantitatively from the two DMBE PESs.[33,40] In order to compare with the experimental values more directly, energies including zero point energy (ZPE) corrections are given in Figure 2 in red color. As shown in Figure 2, the two reactions are highly exoergic. In the reactant channel of R1, interestingly, there is a saddle point (SP) in the entrance channel located between a shallow (0.18 kcal/mol) van der Waals (vdW) minimum and the *cis*-HO_3 minimum, which is 0.86 kcal/mol above the reactant and in excellent agreement with the experimental activation energy of about 0.9 kcal/mol.[71,72] This barrier, which has been noted in some previous *ab initio* calculations,[40,73] has an important implication in kinetics, as discussed below. On the other hand, the R2 reaction is barrierless. Considering the ZPE correction, R1 has a large exoergicity of 77.71 kcal/mol, which is in excellent agreement with the experimental results (77.72 ± 0.06 kcal/mol).[74−76] For R2, the reaction exoergodicity of −52.91 kcal/mol also compares well with the experimental value (−53.77 ± 0.09 kcal/mol).[74,76]

Similar to our earlier semiglobal PES,[52] the new global PES has a global minimum in planar *trans*-HO_3 with a binding energy of 4.01 kcal/mol relative to the OH + O_2 product asymptote, while planar *cis*-HO_3 is located only 0.18 kcal/mol above. The relative stability for the two conformers is consistent with the available evidence.[48] The two conformers are connected by an isomerization saddle point (*iso*-SP) with a barrier height of 1.10 kcal/mol relative to the global minimum.

Two-dimensional contours of the PES in pairs of bond lengths are shown in Figure 3. Figure 3a and b illustrate features of H + O_3 → OH + O_2 and HO_2 + O → OH + O_2 reaction paths, respectively. The vdW well and small barrier can be seen in the H + O_3 channel, as shown in Figure 3a. There are no classical barriers in both reactant and product channels for R2. In Figure 3c, the saddle point *iso*-SP is clearly seen along the isomerization pathway between *trans*-HO_3 and

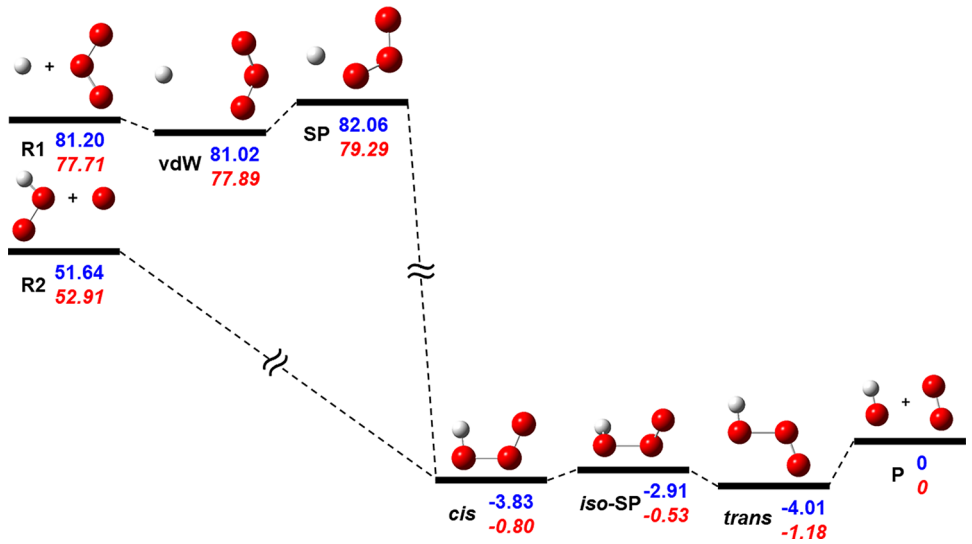

Figure 2. Energetics of the H + O_3 → OH + O_2 and HO_2 + O → OH + O_2 reactions on the $HO_3(^2A'')$ PES. The energies are relative to the OH + O_2 asymptote in kcal/mol. The values indicated by blue are energies of stationary points obtained from the PES, and its corrections with ZPE are shown in red italic.

https://dx.doi.org/10.1021/acs.jpca.0c04321
J. Phys. Chem. A 2020, 124, 6427−6437

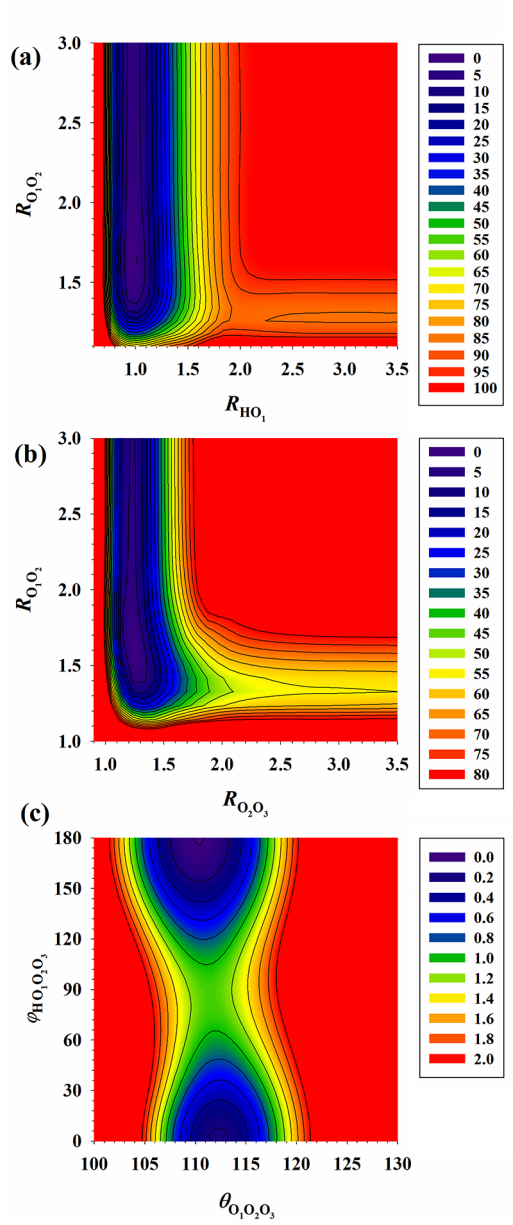

Figure 3. Contour plots for (a) H + O_3 → OH + O_2, (b) HO_2 + O → OH + O_2, and (c) *cis*-HO_3 ↔ *trans*-HO_3 isomerization processes. The other four coordinates are optimized. Energies are in kcal/mol with respect to the *trans*-HO_3 complex.

cis-HO_3. In addition, these contour plots confirm the smoothness of the PES.

Thanks to the high fidelity of the PIP-NN fitting approach, the *ab initio* properties of the stationary points are reproduced well on the PES. The geometries of all stationary points optimized on the PES are listed in Table 1. For comparison, previous theoretical results and available experimental values are also included. The geometries of both reactants and products on the PES agree well with experiments with the discrepancies in bond lengths and angles less than 0.01 Å and 0.6°, respectively. It is found that the geometric parameters, especially the central O_1−O_2 bond lengths of the *cis*-HO_3 and *trans*-HO_3 structures, are very sensitive to the *ab initio* method used.[26,34,77] The geometries predicted by multireference calculations are generally in better agreement with the available experimental data than a single-reference method, suggesting a large multireference character in this system.[26] It should be noted that both SP and vdW minimum have nonplanar structures, which are quite different from the planar geometry of the submerged transition state found on the DMBE I PES[40] but consistent with the out-of-plane geometry obtained from the *ab initio* multiconfiguration Hatree-Fock (MCHF) calculations (see Table 1).[73] The harmonic frequencies of all stationary points were also calculated and summarized in Table 2, comparing to available experimental and theoretical data. It can be seen that our results are in better agreement with the ones calculated at the MRCI-C6/VTZ level than the CCSD(T) results.[26] The nonplanar *iso*-SP has a single imaginary frequency of 156.12*i* cm^{-1}. For the frequencies of two conformers, the agreement with experimental fundamental frequencies obtained by Derro et al.[29] is also quite good, validating the accuracy of the PES in this region. All of these results indicate that the current PIP-NN PES for the HO_3 system should be reliable for dynamical and kinetic studies of the two title reactions.

III.B. Rate Coefficients. Based on the new PES, the thermal rate coefficients of the H + O_3 → OH + O_2 (R1) and HO_2 + O → OH + O_2 (R2) reactions were calculated using the QCT method. Large numbers of trajectories (100000 for $T \leq 600$ K, 50000 for $T > 600$ K) have been calculated at seven specified temperatures over the range from 200 to 2000 K, which are much more than the trajectory numbers run in previous theoretical studies.[46,50] The statistical errors are all within 3.0% except for R1 at 200 K (4.31%). The total energy conserved within 10^{-4} kcal/mol for almost all trajectories, confirming the smoothness of the PES.

The QCT thermal rate coefficients for R1 at various temperatures are summarized in Table 3 along with corresponding statistical errors and are graphically illustrated in Figure 4, together with previous calculated ones[44,45] and available experimental data.[8−12,71] At 298 K, the experimental results lie between 1.5×10^{-11} and 2.85×10^{-11} cm^3/s. The QCT rate coefficient (2.06×10^{-11} cm^3/s) is in the middle of the experimental range and is close to those of Phillips and Schiff[8] ($(2.60 \pm 0.50) \times 10^{-11}$ cm^3/s) and Clyne et al.[9] ($(1.76 \pm 0.21) \times 10^{-11}$ cm^3/s). At lower temperatures, our results are visibly lower than the experimental values. This is partly caused by the neglect of the quantum tunneling effect in the QCT calculations, which generally plays an important role at low temperatures. However, the calculated results have a larger deviation from the data of Clyne et al.[9] at higher temperatures of 479 and 638 K. As shown in Figure 4, the reduced-dimensional quantum rate coefficients[45] carried out on the DMBE I PES by Varandas et al. using the infinite-order sudden-approximation (IOSA) method underestimate the QCT results on both DMBE I PES[44] and our PES by a factor of 5 over the entire temperature range. The large discrepancy can presumably be attributed to the fact that the QD calculations[45] were performed with reduced dimensionality.

We also predicted k_1 at higher temperatures up to 2000 K. Importantly, the calculated k_1 exhibit a positive temperature dependence, which is in good agreement with experiments.[8−12] The positive dependence of the rate coefficient can be attributed to the small barrier along the H + O_3 reaction path on this PES discussed above.

Meanwhile, the calculated k_2 values for reaction HO_2 + O → OH + O_2 between 200 and 2000 K are also listed in Table 3. In Figure 5, the QCT rate coefficients are compared with other

https://dx.doi.org/10.1021/acs.jpca.0c04321
J. Phys. Chem. A 2020, 124, 6427−6437

Table 1. Theoretical and Experimental Geometries of Stationary Points in the HO_3 Reaction System[a]

species	methods	R_{HO_1}	$R_{O_1O_2}$	$R_{O_2O_3}$	$\theta_{HO_1O_2}$	$\theta_{O_1O_2O_3}$	$\varphi_{HO_1O_2O_3}$
H + O_3	this work		1.2813	1.2813		116.64	
	expt.[84]		1.278	1.278		116.8	
vdW	this work	3.1680	1.2800	1.2800	80.63	116.96	66.55
	DMBE I[40]	2.7369	1.2700	1.2700	142.9	116.8	0
SP	this work	2.0244	1.2916	1.2817	95.82	115.56	57.31
	DMBE I[40]	2.3430	1.2621	1.2644	112.77	114.6	0
	MCHF[73]	2.0721	1.3210	1.3124	107.3	112.7	84.8
HO_2 + O	this work	0.9723	1.3401		103.70		
	expt.[85]	0.9707	1.3305		104.29		
cis-HO_3	this work	0.9747	1.5786	1.2442	96.91	112.28	0
	DMBE I[40]	0.9639	1.4335	1.2390	105.3	115.2	0
	DMBE II[33]	0.9773	1.4771	1.2591	97.69	110.24	0
	Theo.1[b]	0.975	1.433	1.243	98.6	111.4	0
	Theo.2[c]	0.97	1.461	1.268	98.6	110.9	0
	Theo.3[d]	0.973	1.503	1.251	99.5	112.6	0
	Theo.4[e]	0.976	1.75	1.229	94.3	113.4	0
	Theo.5[f]	0.9741	1.5041	1.2114	97.08	112.02	0
	Theo.6[g]	0.9715	1.5218	1.2448	97.74	111.68	0
	Theo.7[h]	0.9723	1.5289	1.2445	97.71	111.77	0
	Theo.8[i]	0.9706	1.5195	1.2424	97.8	111.69	0
	Theo.9[j]	0.9715	1.5252	1.2426	97.8	111.77	0
	Theo.10[k]	0.9709	1.5805	1.2443	96.21	111.96	0
	Theo.11[l]	0.9752	1.574	1.2652	98.01	112.69	9.12
	Theo.12[m]	1.2599	1.5752	0.9724	112.85	97.9	0
iso-SP	this work	0.9719	1.6764	1.2301	95.67	111.52	85.50
	Theo.10[k]	0.9685	1.713	1.2238	94.5	112.05	77.64
	Theo.11[l]	0.9719	1.6173	1.2527	97.19	111.29	84.76
	Theo.12[m]	1.2596	1.561	0.9707	111.08	97.68	90.72
trans-HO_3	this work	0.9716	1.6614	1.2243	96.17	110.35	180
	DMBE I[40]	0.9793	1.5069	1.2269	101.5	112.7	180
	DMBE II[33]	0.9632	1.4804	1.2465	101.01	109.87	180
	Theo.1[b]	0.969	1.437	1.241	99.2	109.2	180
	Theo.2[c]	0.966	1.475	1.257	98.7	108.8	180
	Theo.3[d]	0.97	1.544	1.234	98.3	110.3	180
	Theo.4[e]	0.975	1.75	1.223	94.1	111	180
	Theo.5[f]	0.9705	1.5887	1.186	97.43	110.34	180
	Theo.6[g]	0.9684	1.581	1.225	97.43	109.64	180
	Theo.7[h]	0.9693	1.5887	1.2248	97.41	109.7	180
	Theo.8[i]	0.9675	1.578	1.2228	97.5	109.67	180
	Theo.9[j]	0.9686	1.5848	1.2229	97.48	109.68	180
	Theo.10[k]	0.9684	1.6951	1.2203	95.03	110.48	180
	Theo.11[l]	0.9706	1.6187	1.2446	97.15	110.01	180
	Theo.12[m]	1.2446	1.6187	0.9706	110.01	97.15	180
	expt.[31]	0.972	1.688	1.225	90.04	111.02	180
OH + O_2	this work	0.9716		1.2148			
	expt.[86]	0.9697		1.2075			

[a]Bond lengths and angles are in units of angstroms and degrees, respectively. [b]MP2. [c]QCISD. [d]B3LYP. [e]CASSCF. [f]CCSD(T)-C6/V5Z//MP2-C6/V5Z. [g]CCSD(T)-C6/V5Z. [h]CCSD(T)-C6/AVQZ. [i]CCSD(T)-C0/CV5Z. [j]CCSD(T)-C0/ACVQZ. [k]MRCI-C6/VTZ//MRCI-C6/VTZ. [l]2-RDM(M)/AVTZ. [m]2-RDM(M)/VTZ. Theo.1−4, 5−10, and 11−12 are collected from refs 34, 26, and 77, respectively.

theoretical[34,46,47,49,50,78,79] as well as experiment results.[13−23,51,72,80−83] The QCT rate coefficients in this work have a negative temperature dependence and are in satisfactory agreement with the tendency of experimental estimation. This negative temperature dependence is consistent with the barrierless PES for this channel. Our results are between the QCT results calculated on the two DMBE PESs below 300 K with relatively small differences. Due to the severe approximations involved, the two quantum mechanical results[47] show larger discrepancies with the experiments on the trend or numerical values. Most of the experimental measurements are performed at temperatures below 400 K, as displayed in Figure 5. The experimental k_2 values are scattered, for instance, from $(3.1 \pm 1.0) \times 10^{-11}$ cm^3/s of Burrows et al.[16] to $(7 \pm 2) \times 10^{-11}$ cm^3/s of Lii et al.[18] at 298 K. The QCT results on our PES are consistent with early experimental results of Hack et al.[17] and Burrows et al.[15,16] However, later experiments of Nicovich et al.[23] and Keyser et al.[19] reported higher experimental values at room temperature with a stronger negative temperature dependence. There is a weak variation of

https://dx.doi.org/10.1021/acs.jpca.0c04321
J. Phys. Chem. A 2020, 124, 6427−6437

Table 2. Calculated Harmonic Frequencies (cm^{-1}) of Stationary Points in the HO_3 Reaction System[a]

species	method	harmonic frequencies					
H + O_3	this work	1108.73	1068.93	694.25			
	expt.[84]	1134.9	1089.2	716.0			
vdW	this work	1115.84	1071.78	691.72	141.03	51.78	49.14
SP	this work	1143.77	1045.97	715.37	376.87	98.00	729.13 *i*
HO_2 + O	this work	3658.68	1431.88	1116.68			
	expt.[87]	3436.20	1391.75	1097.63			
cis-HO_3	this work	3728.13	1361.28	1220.05	608.01	306.14	212.95
	Theo.1[b]	3703.48	1393.32	1244.53	656.90	400.69	188.14
	Theo.2[c]	3696.72	1387.02	1240.50	651.51	392.18	149.99
	Theo.3[d]	3716.52	1398.16	1248.29	661.02	408.27	230.52
	Theo.4[e]	3680.92	1374.88	1228.07	645.79	384.45	186.54
	Theo.5[f]	3721.68	1356.04	1221.63	595.66	282.17	238.54
	Theo.6[g]	3630.43	1452.61	1167.89	779.94	414.63	352.46
	expt.[29]	3565		1008.6	486.5	243.6	149.1
iso-SP	this work	3756.09	1382.48	1076.83	534.69	229.88	156.12 *i*
	Theo.6[g]	3843.99	1353.19	1015.18	480.72	111.52	
trans-HO_3	this work	3757.72	1442.01	1110.80	519.85	292.16	174.98
	Theo.1[b]	3756.53	1377.39	1211.21	594.60	356.22	82.86
	Theo.2[c]	3749.82	1376.75	1204.81	588.81	349.54	111.83
	Theo.3[d]	3769.62	1379.61	1213.41	595.75	355.94	104.46
	Theo.4[e]	3731.11	1361.48	1196.83	583.43	346.92	132.99
	Theo.5[f]	3761.91	1421.35	1094.27	501.41	222.04	147.61
	Theo.6[g]	3727.83	1424.94	979.58	450.07	133.92	78.67
	expt.[29]	3569.3		997.9	481.9	243.7	128.7
OH + O_2	this work	3763.69	1553.78				
	expt.[86]	3737.76	1580.19				

[a]The experimental fundamentals are included in comparison. [b]CCSD(T)-C6/V5Z. [c]CCSD(T)-C6/AVQZ. [d]CCSD(T)-C0/CVQZ. [e]CCSD(T)-C0/ACVTZ. [f]MRCI-C6/VTZ. [g]2-RDM(M)/VDZ. Theo.1−5 and 6 are collected from refs 26 and 77, respectively.

Table 3. QCT Rate Coefficients for H + O_3 → OH + O_2 and HO_2 + O → OH + O_2 Reactions

	H + O_3 → OH + O_2		HO_2 + O → OH + O_2	
T (K)	k_1 (cm^3/s)	statistical error (%)	k_2 (cm^3/s)	statistical error (%)
200	7.05×10^{-12}	4.31	4.34×10^{-11}	0.49
298	2.06×10^{-11}	2.61	4.04×10^{-11}	0.56
400	3.95×10^{-11}	1.89	3.86×10^{-11}	0.63
600	7.55×10^{-11}	1.35	3.39×10^{-11}	0.98
800	1.16×10^{-10}	1.53	2.95×10^{-11}	1.09
1000	1.53×10^{-10}	1.33	2.50×10^{-11}	1.23
1500	2.60×10^{-10}	1.47	2.22×10^{-11}	1.36
2000	3.98×10^{-10}	1.27	2.25×10^{-11}	1.40

the QCT rate coefficient with temperature above 1000 K, but the experimental data are sparse and diverging. It should be noted that no excited state is considered in the present work, and this may turn out to be significant at high temperatures. Although the overall agreement with kinetic experiments is achieved, it is clear that further improvements are still needed to give a quantitatively accurate description of the title system. These improvements include both a higher level *ab initio* treatment of the entrance channels and quantum dynamics to better describe quantum effects such as tunneling, particularly for R1.

IV. CONCLUSIONS

We report here a new full-dimensional global PES for the ground state of the HO_3 system which covers the interaction region and all three arrangement channels of OH + O_2, H + O_3, and HO_2 + O. The state-of-the-art PES was fitted to more than 21000 *ab initio* points at the level of MRCI-F12/VDZ-F12 using the PIP-NN method. The small total RMSE of the PES indicates a faithful representation of the *ab initio* points. The PES provides a reliable platform for kinetic and dynamical studies, using various classical and quantum methods. Extensive QCT calculations have been carried out on the PES. The thermal rate coefficients for both H + O_3 → OH + O_2 and HO_2 + O → OH + O_2 reactions agree reasonably well with most available experimental results, given the uncertainties in the experimental data. The positive and negative temperature dependences of the two reactions are reproduced

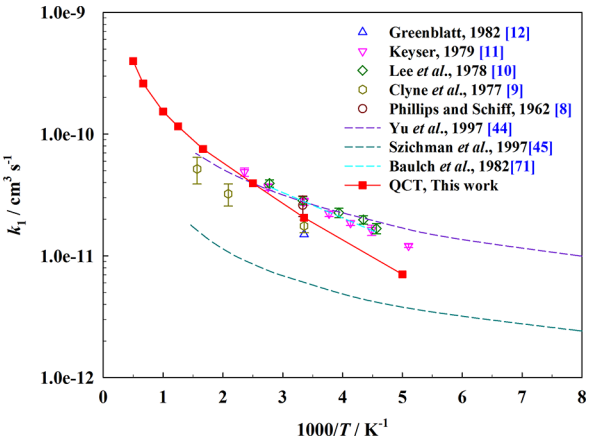

Figure 4. Theoretical[44,45] and experimental[8−12,71] thermal rate coefficients as a function of temperature for the H + O_3 → OH + O_2 reaction.

https://dx.doi.org/10.1021/acs.jpca.0c04321
J. Phys. Chem. A 2020, 124, 6427−6437

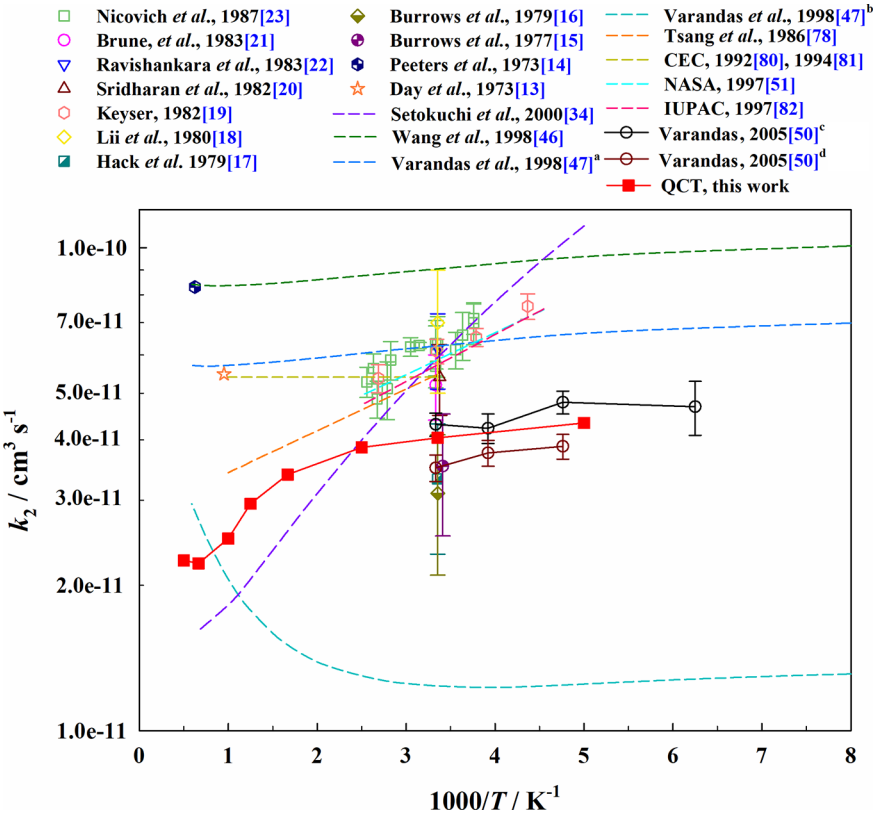

Figure 5. Theoretical[34,46,47,49,50,78,79] and experimental[13−23,51,72,80−83] thermal rate coefficients as a function of temperature for the $HO_2 + O \rightarrow OH + O_2$ reaction. Notes: [a]Reduced dimensional QD results. [b]Reduced dimensional QD results on DMBE I PES. [c]QCT on DMBE I PES. [d]QCT on DMBE II PES.

and their origins revealed. We hope our theoretical investigations reported in this work will motivate further dynamic calculations and new experiments, thus shedding further light on these important reactions. In particular, an in-depth investigation on product distributions and the effect of vibrational excitation on the dynamics and kinetics for the title reactions will shed further light on the role of these reactions in atmospheric chemistry and combustion. Such studies are underway in our group and will be reported in the near future.

AUTHOR INFORMATION

Corresponding Authors

Xixi Hu − *Kuang Yaming Honors School, Nanjing University, Nanjing 210023, China;* orcid.org/0000-0003-1530-3015; Email: xxhu@nju.edu.cn

Daiqian Xie − *Institute of Theoretical and Computational Chemistry, Key Laboratory of Mesoscopic Chemistry, School of Chemistry and Chemical Engineering, Nanjing University, Nanjing 210093, China;* orcid.org/0000-0001-7185-7085; Email: dqxie@nju.edu.cn

Authors

Junxiang Zuo − *Institute of Theoretical and Computational Chemistry, Key Laboratory of Mesoscopic Chemistry, School of Chemistry and Chemical Engineering, Nanjing University, Nanjing 210093, China; Department of Chemistry and Chemical Biology, University of New Mexico, Albuquerque, New Mexico 87131;* orcid.org/0000-0002-2967-125X

Qixin Chen − *Institute of Theoretical and Computational Chemistry, Key Laboratory of Mesoscopic Chemistry, School of Chemistry and Chemical Engineering, Nanjing University, Nanjing 210093, China*

Hua Guo − *Department of Chemistry and Chemical Biology, University of New Mexico, Albuquerque, New Mexico 87131;* orcid.org/0000-0001-9901-053X

Complete contact information is available at: https://pubs.acs.org/10.1021/acs.jpca.0c04321

Author Contributions

[‖]J.Z., Q.C.: These authors contributed equally.

Notes

The authors declare no competing financial interest.

ACKNOWLEDGMENTS

This work was supported by National Natural Science Foundation of China (Grant No. U1932147 to X.H., Grant Nos. 21733006 and 21590802 to D. X.), by US Department of Energy (Grant No. DE-SC0015997 to H.G.), and the Fundamental Research Funds for the Central Universities (Grant No. 14380016 to X.H.).

REFERENCES

(1) Varandas, A. J. C. Four-Atom Bimolecular Reactions with Relevance in Environmental Chemistry: Theoretical Work. *Int. Rev. Phys. Chem.* **2000**, *19*, 199−245.

(2) Burke, M. P.; Chaos, M.; Ju, Y.; Dryer, F. L.; Klippenstein, S. J. Comprehensive H_2/O_2 Kinetic Model for High-Pressure Combustion. *Int. J. Chem. Kinet.* **2012**, *44*, 444−474.

(3) Suma, K.; Sumiyoshi, Y.; Endo, Y. The Rotational Spectrum and Structure of the HOOO Radical. *Science* **2005**, *308*, 1885−1886.

(4) Murray, C.; Derro, E. L.; Sechler, T. D.; Lester, M. I. Weakly Bound Molecules in the Atmosphere: A Case Study of HOOO. *Acc. Chem. Res.* **2009**, *42*, 419−427.
(5) Holloway, A. M.; Wayne, R. P. *Atmospheric Chemistry*; Royal Society of Chemistry: 2015.
(6) Crutzen, P. Mesospheric Mysteries. *Science* **1997**, *277*, 1951−1952.
(7) Srinivasan, N. K.; Su, M. C.; Sutherland, J. W.; Michael, J. V. Reflected Shock Tube Studies of High-Temperature Rate Constants for $CH_3 + O_2$, $H_2CO + O_2$, and $OH + O_2$. *J. Phys. Chem. A* **2005**, *109*, 7902−7914.
(8) Phillips, L. F.; Schiff, H. I. Mass Spectrometric Studies of Atomic Reactions. III. Reactions of Hydrogen Atoms with Nitrogen Dioxide and with Ozone. *J. Chem. Phys.* **1962**, *37*, 1233−1238.
(9) Clyne, M. A.; Monkhouse, P. B. Atomic Resonance Fluorescence for Rate Constants of Rapid Bimolecular Reactions. Part 5—Hydrogen Atom Reactions; H+ NO_2 and H+O_3. *J. Chem. Soc., Faraday Trans. 2* **1977**, *73*, 298−309.
(10) Lee, J.; Michael, J.; Payne, W.; Stief, L. Absolute Rate of the Reaction of Hydrogen Atoms with Ozone from 219−360 K. *J. Chem. Phys.* **1978**, *69*, 350−354.
(11) Keyser, L. Absolute Rate Constant and Temperature Dependence of the Reaction between Hydrogen (^{2}S) Atoms and Ozone. *J. Phys. Chem.* **1979**, *83*, 645−648.
(12) Greenblatt, G. D.; Wiesenfeld, J. R. Time-Resolved Emission Studies of Vibrationally Excited Hydroxyl Radicals: OH ($X^2\Pi$, v″ = 9). *J. Geophys. Res.* **1982**, *87*, 11145−11152.
(13) Day, M. J.; Thompson, K.; Dixon-Lewis, G. Some Reactions of Hydroperoxyl and Hydroxyl Radicals at High Temperatures. *Symp. (Int.) Combust., [Proc.]* **1973**, *14*, 47−59.
(14) Peeters, J.; Mahnen, G. Reaction Mechanisms and Rate Constants of Elementary Steps in Methane-Oxygen Flames. *Symp. (Int.) Combust., [Proc.]* **1973**, *14*, 133−146.
(15) Burrows, J.; Harris, G.; Thrush, B. Rates of Reaction of HO_2 with HO and O Studied by Laser Magnetic Resonance. *Nature* **1977**, *267*, 233−234.
(16) Burrows, J. P.; Cliff, D. I.; Harris, G. W.; Thrush, B. A.; Wilkinson, J. P. T. Atmospheric Reactions of the HO_2 Radical Studied by Laser Magnetic-Resonance Spectroscopy. *Proc. R. Soc. London Ser. A* **1979**, *368*, 463−481.
(17) Hack, W.; Preuss, A. W.; Temps, F.; Wagner, H. G. The Reaction $O + HO_2 \rightarrow OH + O_2$ Studied with a LMR-ESR-Spectrometer. *Ber. Bunsenges. Phys. Chem.* **1979**, *83*, 1275−1279.
(18) Lii, R. R.; Sauer, M. C., Jr.; Gordon, S. Rate Constant of the Reaction of $O(^3P)$ with HO_2. *J. Phys. Chem.* **1980**, *84*, 817−819.
(19) Keyser, L. F. Kinetics of the Reaction $O + HO_2 \rightarrow OH + O_2$ from 229 to 372 K. *J. Phys. Chem.* **1982**, *86*, 3439−3446.
(20) Sridharan, U.; Qiu, L.; Kaufman, F. Kinetics and Product Channels of the Reactions of HO_2 with O and H Atoms at 296 K. *J. Phys. Chem.* **1982**, *86*, 4569−4574.
(21) Brune, W. H.; Schwab, J. J.; Anderson, J. Laser Magnetic Resonance, Resonance Fluorescence, Resonance Absorption Studies of the Reaction Kinetics of $O + OH \rightarrow H + O_2$, $O + HO_2 \rightarrow OH + O_2$, $N + OH \rightarrow H + NO$, and $N + HO_2 \rightarrow$ Products at 300 K between 1 and 5 Torr. *J. Phys. Chem.* **1983**, *87*, 4503−4514.
(22) Ravishankara, A.; Wine, P.; Nicovich, J. Pulsed Laser Photolysis Study of the Reaction Between $O(^3P)$ and HO_2. *J. Chem. Phys.* **1983**, *78*, 6629−6639.
(23) Nicovich, J.; Wine, P. Temperature Dependence of the O + HO_2 Rate Coefficient. *J. Phys. Chem.* **1987**, *91*, 5118−5123.
(24) Suma, K.; Sumiyoshi, Y.; Endo, Y. Force-Field Calculation and Geometry of the HOOO Radical. *J. Chem. Phys.* **2013**, *139*, 094301.
(25) Varandas, A. J. C. Ab Initio Treatment of Bond-Breaking Reactions: Accurate Course of HO_3 Dissociation and Revisit to Isomerization. *J. Chem. Theory Comput.* **2012**, *8*, 428−441.
(26) Varandas, A. J. C. Is HO_3 Minimum cis or trans? An Analytic Full-Dimensional *Ab Initio* Isomerization Path. *Phys. Chem. Chem. Phys.* **2011**, *13*, 9796−9811.
(27) Anglada, J. M.; Olivella, S.; Solé, A. On the Dissociation of Ground State trans-HOOO Radical: A Theoretical Study. *J. Chem. Theory Comput.* **2010**, *6*, 2743−2750.
(28) Varner, M. E.; Harding, M. E.; Vázquez, J.; Gauss, J.; Stanton, J. F. Dissociation Energy of the HOOO Radical. *J. Phys. Chem. A* **2009**, *113*, 11238−11241.
(29) Derro, E. L.; Sechler, T. D.; Murray, C.; Lester, M. I. Observation of $\nu_1+\nu_n$ Combination Bands of the HOOO and DOOO Radicals Using Infrared Action Spectroscopy. *J. Chem. Phys.* **2008**, *128*, 244313.
(30) Braams, B. J.; Yu, H. G. Potential Energy Surface and Quantum Dynamics Study of Rovibrational States for HO_3 (X^2A''). *Phys. Chem. Chem. Phys.* **2008**, *10*, 3150−3155.
(31) Mansergas, A.; Anglada, J. M.; Olivella, S.; Ruiz-Lopez, M. F.; Martins-Costa, M. On the Nature of the Unusually Long OO Bond in HO_3 and HO_4 Radicals. *Phys. Chem. Chem. Phys.* **2007**, *9*, 5865−5873.
(32) Fabian, W. M. F.; Kalcher, J.; Janoschek, R. Stationary Points on the Energy Hypersurface of the Reaction O_3+H·→ (·O_3H)* ↔ O_2 +·OH and Thermodynamic Functions of ·O_3H at G3MP2B3, CCSD(T)-CBS (W1U) and MR-ACPF-CBS Levels of Theory. *Theor. Chem. Acc.* **2005**, *114*, 182−188.
(33) Yu, H. G.; Varandas, A. J. C. Ab Initio Theoretical Calculation and Potential Energy Surface for Ground-State HO_3. *Chem. Phys. Lett.* **2001**, *334*, 173−178.
(34) Setokuchi, O.; Sato, M.; Matuzawa, S. A Theoretical Study of the Potential Energy Surface and Rate Constant for an $O(^3P) + HO_2$ Reaction. *J. Phys. Chem. A* **2000**, *104*, 3204−3210.
(35) Zuo, J. X.; Hu, X. X.; Xie, D. Q. Quantum Dynamics of Oxyhydrogen Complex-Forming Reactions for the HO_2 and HO_3 Systems. *Chin. J. Chem. Phys.* **2018**, *31*, 123−134.
(36) Varner, M. E.; Harding, M. E.; Gauss, J.; Stanton, J. F. On the Geometry of the HO_3 Radical. *Chem. Phys.* **2008**, *346*, 53−55.
(37) Denis, P. A.; Ornellas, F. R. Theoretical Characterization of Hydrogen Polyoxides: HOOH, HOOOH, HOOOOH, and HOOO. *J. Phys. Chem. A* **2009**, *113*, 499−506.
(38) McCarthy, M. C.; Lattanzi, V.; Kokkin, D.; Martinez, O., Jr.; Stanton, J. F. On the Molecular Structure of HOOO. *J. Chem. Phys.* **2012**, *136*, 034303.
(39) Varandas, A. J. C. Odd-Hydrogen: An Account on Electronic Structure, Kinetics, and Role of Water in Mediating Reactions with Atmospheric Ozone. Just a Catalyst or Far Beyond? *Int. J. Quantum Chem.* **2014**, *114*, 1327−1349.
(40) Varandas, A. J. C.; Yu, H. G. Double Many-Body Expansion Potential Energy Surface for Ground-State HO_3. *Mol. Phys.* **1997**, *91*, 301−318.
(41) Speranza, M. Structure, Stability, and Reactivity of Cationic Hydrogen Trioxides and Thermochemistry of Their Neutral Analogs. A Fourier-Transform Ion Cyclotron Resonance Study. *Inorg. Chem.* **1996**, *35*, 6140−6151.
(42) Cacace, F.; de Petris, G.; Pepi, F.; Troiani, A. Experimental Detection of Hydrogen Trioxide. *Science* **1999**, *285*, 81−82.
(43) Le Picard, S. D.; Tizniti, M.; Canosa, A.; Sims, I. R.; Smith, I. W. M. The Thermodynamics of the Elusive HO_3 Radical. *Science* **2010**, *328*, 1258−1262.
(44) Yu, H. G.; Varandas, A. J. C. Dynamics of H(D) + O_3 Reactions on a Double Many-Body Expansion Potential-Energy Surface for Ground State HO_3. *J. Chem. Soc., Faraday Trans.* **1997**, *93*, 2651−2656.
(45) Szichman, H.; Baer, M.; Varandas, A. J. C. Quantum Dynamical Rate Constant for the H + O_3 Reaction Using a Six-Dimensional Double Many-Body Expansion Potential Energy Surface. *J. Phys. Chem. A* **1997**, *101*, 8817−8821.
(46) Wang, W.; González-Jonte, R.; Varandas, A. J. C. Quasiclassical Trajectory Study of the Environmental Reaction $O + HO_2 \rightarrow OH + O_2$. *J. Phys. Chem. A* **1998**, *102*, 6935−6941.
(47) Varandas, A. J. C.; Szichman, H. A Three-Dimensional Quantum Mechanical Study of the O+HO_2 Atmospheric Reaction: Infinite-Order Sudden Approximation and Novel Adiabatic Ap-

https://dx.doi.org/10.1021/acs.jpca.0c04321
J. Phys. Chem. A 2020, 124, 6427−6437

proaches vs. Quasiclassical Trajectories. *Chem. Phys. Lett.* **1998**, *295*, 113−121.
(48) Beames, J. M.; Lester, M. I.; Murray, C.; Varner, M. E.; Stanton, J. F. Analysis of the HOOO Torsional Potential. *J. Chem. Phys.* **2011**, *134*, 044304.
(49) Silveira, D. M.; Caridade, P. J. S. B.; Varandas, A. J. C. Dynamics Study of the O + HO_2 Reaction Using Two DMBE Potential Energy Surfaces: The Role of Vibrational Excitation. *J. Phys. Chem. A* **2004**, *108*, 8721−8730.
(50) Varandas, A. J. C. What are the Implications of Nonequilibrium in the O+OH and O+HO_2 Reactions? *ChemPhysChem* **2005**, *6*, 453−465.
(51) DeMore, W. B.; Sander, S. P.; Golden, D. M.; Molina, M. J.; Hampson, R. F.; Kurylo, M. J.; Howard, C. J.; Kolb, C. E.; Ravishankara, A. R. *Chemical Kinetics and Photochemical Data for Use in Stratospheric Modelling, Evaluation Number 12*; JPL Publication: 1997.
(52) Hu, X.; Zuo, J.; Xie, C.; Dawes, R.; Guo, H.; Xie, D. An Ab Initio Based Full-Dimensional Potential Energy Surface for OH + O_2 ⇄ HO_3 and Low-Lying Vibrational Levels of HO_3. *Phys. Chem. Chem. Phys.* **2019**, *21*, 13766−13775.
(53) Behler, J. Neural Network Potential-Energy Surfaces in Chemistry: A Tool for Large-Scale Simulations. *Phys. Chem. Chem. Phys.* **2011**, *13*, 17930−17955.
(54) Raff, L. M.; Komanduri, R.; Hagan, M.; Bukkapatnam, S. T. S. *Neural Networks in Chemical Reaction Dynamics*; Oxford University Press: 2012.
(55) Jiang, B.; Li, J.; Guo, H. Potential Energy Surfaces from High Fidelity Fitting of Ab Initio Points: the Permutation Invariant Polynomial-Neural Network Approach. *Int. Rev. Phys. Chem.* **2016**, *35*, 479−506.
(56) Werner, H. J.; Knowles, P. J.; Knizia, G.; Manby, F. R.; Schütz, M. Molpro: A General-Purpose Quantum Chemistry Program Package. *Wiley Interdiscip. Rev. Comput. Mol. Sci.* **2012**, *2*, 242−253.
(57) Deskevich, M. P.; Nesbitt, D. J.; Werner, H.-J. Dynamically Weighted Multiconfiguration Self-Consistent Field: Multistate Calculations for F + H_2O → HF + OH Reaction Paths. *J. Chem. Phys.* **2004**, *120*, 7281−7289.
(58) Dawes, R.; Jasper, A. W.; Tao, C.; Richmond, C.; Mukarakate, C.; Kable, S. H.; Reid, S. A. Theoretical and Experimental Spectroscopy of the S_2 State of CHF and CDF: Dynamically Weighted Multireference Configuration Interaction Calculations for High-Lying Electronic States. *J. Phys. Chem. Lett.* **2010**, *1*, 641−646.
(59) Shiozaki, T.; Knizia, G.; Werner, H.-J. Explicitly Correlated Multireference Configuration Interaction: MRCI-F12. *J. Chem. Phys.* **2011**, *134*, 034113.
(60) Peterson, K. A.; Adler, T. B.; Werner, H.-J. Systematically Convergent Basis Sets for Explicitly Correlated Wavefunctions: The atoms H, He, B-Ne, and Al-Ar. *J. Chem. Phys.* **2008**, *128*, 084102.
(61) Langhoff, S. R.; Davidson, E. R. Configuration Interaction Calculations on the Nitrogen Molecule. *Int. J. Quantum Chem.* **1974**, *8*, 61−72.
(62) Jiang, B.; Guo, H. Permutation Invariant Polynomial Neural Network Approach to Fitting Potential Energy Surfaces. *J. Chem. Phys.* **2013**, *139*, 054112.
(63) Li, J.; Jiang, B.; Guo, H. Permutation Invariant Polynomial Neural Network Approach to Fitting Potential Energy Surfaces. II. Four-Atom Systems. *J. Chem. Phys.* **2013**, *139*, 204103.
(64) Braams, B. J.; Bowman, J. M. Permutationally Invariant Potential Energy Surfaces in High Dimensionality. *Int. Rev. Phys. Chem.* **2009**, *28*, 577−606.
(65) Hagan, M. T.; Menhaj, M. B. Training Feedforward Networks with the Marquardt Algorithm. *IEEE Trans. Neural Netw.* **1994**, *5*, 989−993.
(66) Hu, X.; Hase, W. L.; Pirraglia, T. Vectorization of the General Monte Carlo Classical Trajectory Program VENUS. *J. Comput. Chem.* **1991**, *12*, 1014−1024.
(67) Hase, W. L.; Duchovic, R. J.; Hu, X.; Komornicki, A.; Lim, K. F.; Lu, D. H.; Peslherbe, G. H.; Swamy, K. N.; Vande Linde, S. R. R.; Varandas, A. VENUS96: A General Chemical Dynamics Computer Program. *J. Quantum Chem. Program Exch. Bull.* **1996**, *16*, 671.
(68) Zuo, J.; Chen, Q.; Hu, X.; Guo, H.; Xie, D. Dissection of the Multichannel Reaction of Acetylene with Atomic Oxygen: From the Global Potential Energy Surface to Rate Coefficients and Branching Dynamics. *Phys. Chem. Chem. Phys.* **2019**, *21*, 1408−1416.
(69) Lu, D.-d.; Xie, C.-j.; Li, J.; Guo, H. Rate Coefficients and Branching Ratio for Multi-Channel Hydrogen Abstractions from CH3OH by F. *Chin. J. Chem. Phys.* **2019**, *32*, 84−88.
(70) Guo, Y.; Thompson, D. L.; Sewell, T. D. Analysis of the Zero-Point Energy Problem in Classical Trajectory Simulations. *J. Chem. Phys.* **1996**, *104*, 576−582.
(71) Baulch, D. L.; Cox, R. A.; Crutzen, P. J.; Hampson, R. F., Jr.; Kerr, J. A.; Troe, J.; Watson, R. T. Evaluated Kinetic and Photochemical Data for Atmospheric Chemistry: Supplement I CODATA Task Group on Chemical Kinetics. *J. Phys. Chem. Ref. Data* **1982**, *11*, 327−496.
(72) Atkinson, R.; Baulch, D.; Cox, R.; Hampson, R., Jr.; Kerr, J.; Troe, J. Evaluated Kinetic and Photochemical Data for Atmospheric Chemistry: Supplement IV. IUPAC Subcommittee on Gas Kinetic Data Evaluation for Atmospheric Chemistry. *J. Phys. Chem. Ref. Data* **1992**, *21*, 1125−1568.
(73) Dupuis, M.; Fitzgerald, G.; Hammond, B.; Lester, W. A., Jr.; Schaefer III, H. F. Theoretical study of the H+O_3↔OH+O_2↔O +HO_2 system. *J. Chem. Phys.* **1986**, *84*, 2691−2697.
(74) Cox, J. D.; Wagman, D. D.; Medvedev, V. A. *CODATA Key Values for Thermodynamics*; Hemisphere Publishing Corporation: New York, Washington, Philadelphia, London, 1989.
(75) Taniguchi, N.; Takahashi, K.; Matsumi, Y.; Dylewski, S. M.; Geiser, J. D.; Houston, P. L. Determination of the Heat of Formation of O_3 Using Vacuum Ultraviolet Laser-Induced Fluorescence Spectroscopy and Two-Dimensional Product Imaging Techniques. *J. Chem. Phys.* **1999**, *111*, 6350−6355.
(76) Ruscic, B.; Pinzon, R. E.; Morton, M. L.; Srinivasan, N. K.; Su, M.-C.; Sutherland, J. W.; Michael, J. V. Active Thermochemical Tables: Accurate Enthalpy of Formation of Hydroperoxyl Radical, HO_2. *J. Phys. Chem. A* **2006**, *110*, 6592−6601.
(77) Hoy, E. P.; Schwerdtfeger, C. A.; Mazziotti, D. A. Relative Energies and Geometries of the cis-and trans-HO_3 Radicals from the Parametric 2-Electron Density Matrix Method. *J. Phys. Chem. A* **2013**, *117*, 1817−1825.
(78) Tsang, W.; Hampson, R. F. Chemical Kinetic Data Base for Combustion Chemistry. Part I. Methane and Related Compounds. *J. Phys. Chem. Ref. Data* **1986**, *15*, 1087−1279.
(79) Baulch, D. L.; Bowman, C. T.; Cobos, C. J.; Cox, R. A.; Just, T.; Kerr, J. A.; Pilling, M. J.; Stocker, D.; Troe, J.; Tsang, W.; Walker, R. W.; Warnatz, J. Evaluated Kinetic Data for Combustion Modeling: Supplement II. *J. Phys. Chem. Ref. Data* **2005**, *34*, 757−1397.
(80) Baulch, D. L.; Cobos, C. J.; Cox, R. A.; Esser, C.; Frank, P.; Just, T.; Kerr, J. A.; Pilling, M. J.; Troe, J.; Walker, R. W.; Warnatz, J. Evaluation of Kinetic Data for Combustion Modelling. *J. Phys. Chem. Ref. Data* **1992**, *21*, 411−734.
(81) Baulch, D. L.; Cobos, C. J.; Cox, R. A.; Frank, P.; Hayman, G.; Just, T.; Kerr, J. A.; Murrells, T.; Pilling, M. J.; Troe, J.; Walker, R. W.; Warnatz, J. Evaluated Kinetic Data for Combustion Modeling. Supplement I. *J. Phys. Chem. Ref. Data* **1994**, *23*, 847−848.
(82) Atkinson, R.; Baulch, D.; Cox, R.; Hampson Jr, R.; Kerr, J.; Rossi, M.; Troe, J. Evaluated Kinetic, Photochemical and Heterogeneous Data for Atmospheric Chemistry: Supplement V. IUPAC Subcommittee on Gas Kinetic Data Evaluation for Atmospheric Chemistry. *J. Phys. Chem. Ref. Data* **1997**, *26*, 521−1011.
(83) Atkinson, R.; Baulch, D.; Cox, R.; Hampson Jr, R.; Kerr, J.; Rossi, M.; Troe, J. Kinetic and photochemical data for atmospheric chemistry, Organic Species: Supplement VII. *J. Phys. Chem. Ref. Data* **1999**, *28*, 191−393.
(84) Herzberg, G. *Molecular Spectra and Molecular Structure: III. Electronic Spectra and Electronic Structure of Polyatomic Molecules*; Krieger Publishing Company: 1966.

https://dx.doi.org/10.1021/acs.jpca.0c04321
J. Phys. Chem. A 2020, 124, 6427−6437

(85) Lubic, K. G.; Amano, T.; Uehara, H.; Kawaguchi, K.; Hirota, E. The ν_1 Band of the DO_2 Radical by Difference Frequency Laser and Diode Laser Spectroscopy: The Equilibrium Structure of the Hydroperoxyl Radical. *J. Chem. Phys.* **1984**, *81*, 4826−4831.
(86) Huber, K. P.; Herzberg, G. *Molecular Spectra and Molecular Structure: IV. Constants of Diatomic Molecules*; Springer Science & Business Media: 1979.
(87) Jacox, M. E. Vibrational and Electronic Energy Levels of Polyatomic Transient Molecules. Supplement A. *J. Phys. Chem. Ref. Data* **1990**, *19*, 1387−1546.

https://dx.doi.org/10.1021/acs.jpca.0c04321
J. Phys. Chem. A 2020, 124, 6427−6437